



OPEN Modeling Urotropine adsorption thermodynamic on kaolinite particles

Qingling Zhu¹✉, Zahra Sabah Ghnim², Subhash Chandra³✉, Jayanti Makasana⁴, Subbulakshmi Ganesan⁵, Aman Shankhyan⁶, M. Ravi Kumar⁷, Girish Chandra Sharma⁸, Ayat Hussein Adhab⁹, Morug Salih Mahdi¹⁰, Aseel Salah Mansoor¹¹, Usama Kadem Radi¹², Nasr Saadoun Abd¹³, Khaled Herati¹⁴✉ & Khursheed Muzammil¹⁵

This research looked at how much Urotropine can be adsorbed by kaolinite particles and the thermodynamics of that process. Since Urotropine is important for gel injections and stabilizing clay, understanding how it adsorbs onto clay can help us accurately model various related processes. Initially, X-ray diffraction (XRD) analysis was conducted on kaolinite samples, verifying their high purity (97%) and correct crystal structure. Subsequent experiments focused on the adsorption of Urotropine from solutions of varying concentrations onto the kaolinite particles. By monitoring Urotropine's concentration in the aqueous solution with a UV device, we observed that kaolinite efficiently adsorbs Urotropine, reaching an adsorption capacity of 112 mg/g. Notably, the Langmuir adsorption isotherm model provided the best fit for predicting this Urotropine adsorption behavior. Further experiments at elevated temperatures, coupled with thermodynamic modeling, revealed an enthalpy of 9534 J/ mole, confirming the endothermic nature of the adsorption. The consistently negative Gibbs free energy (ΔG°) across all temperatures indicated that Urotropine adsorption on kaolinite is spontaneous. Core flooding experiments, using a 10⁵ ppm Urotropine solution injected into kaolinite sand-packs, also confirmed the endothermic reaction. However, these experiments showed a significantly lower adsorption capacity compared to batch experiments. This reduction is attributed to the complexity of the porous media and the presence of inaccessible adsorption sites within the sand-packs.

Keywords Urotropine, Kaolinite, Adsorption capacity, Adsorption thermodynamic

Abbreviations

ARE	Absolute relative error
ASE	Absolute sum of errors
UV	Ultraviolet
XRD	X-ray diffraction

List of symbols

Ce	Equilibrium concentration (g/L)
Ci	Initial concentration (g/L)
G	Gibbs free energy

¹Nanjing Forestry University, Nanjing 210037, Jiangsu, China. ²College of Pharmacy, Alnoor University, Nineveh, Iraq. ³Department of Electrical Engineering, GLA University, Mathura 281406, India. ⁴Department of Chemistry, Faculty of Science, Marwadi University Research Center, Marwadi University, Rajkot, Gujarat 360003, India. ⁵Department of Chemistry and Biochemistry, School of Sciences, JAIN (Deemed to Be University), Bangalore, Karnataka, India. ⁶Centre for Research Impact & Outcome, Chitkara University Institute of Engineering and Technology, Punjab, Chitkara University, Rajpura 140401, India. ⁷Department of Chemistry, Raghu Engineering College, Visakhapatnam, Andhra Pradesh 531162, India. ⁸Department of Applied Sciences-Chemistry, NIMS Institute of Engineering & Technology, NIMS University Rajasthan, Jaipur, India. ⁹Department of Pharmacy, Al-Zahravi University College, Karbala, Iraq. ¹⁰College of MLT, Ahl Al Bayt University, Karbala, Iraq. ¹¹Gilgamesh Ahliya University, Baghdad, Iraq. ¹²Collage of Pharmacy, National University of Science and Technology, Nasiriyah, Dhi Qar 64001, Iraq. ¹³Medical Technical College, Al-Farahidi University, Baghdad, Iraq. ¹⁴Engineering Department, Herat University, Herat, Afghanistan. ¹⁵Department of Public Health, College of Applied Medical Sciences, Khamis Mushait Campus, King Khalid University, 62561 Abha, Saudi Arabia. ✉email: zql1562137418@163.com; subhash.chandra@gla.ac.in; Kh.h1992huni@gmail.com

H	Enthalpy
KD	Thermodynamic equilibrium constant
Kf	Freundlich equilibrium constant
KL	Langmuir equilibrium constant
KT	Temkin equilibrium constant
qe	Adsorption (mg/g-rock)
qo	Adsorption capacity (mg/g-rock)
R	Universal gas constant
R2	Correlation coefficient
S	Entropy
Vs	Solution volume (L)

Today, global oil demand has forced oil companies to produce and maintain mature reservoirs^{1–4}. These reservoirs are usually associated with the problem of pressure drop and excess water production^{5–9}. To solve the pressure drop problem, a significant amount of water is usually injected into the oil reservoirs or aquifers, increasing excess water production^{10–13}. Various methods are used to reduce water cuts, including in-situ gel injection^{14–19}. In this method, the mixture of polymer, crosslinker, or any other additive is prepared on the surface of the earth (which is called gelant), and before turning into a gel, it is injected into a water injection well or an oil production well that has the problem of producing excess water^{9,20–24}.

This method significantly reduces excess water production if the gelant is designed correctly and a firm and durable gel is achieved^{15,25–29}. However, designing and achieving a stable gel has different challenges. One of these challenges is the adsorption of polymer and crosslinker on formation rock particles, which reduces its concentration in the gelant and reaches areas far from the well^{19,30–34}. In this case, some amount of crosslinker will be adsorbed to the surface of the rock, and when it reaches the target area, its composition will change and will not be following the optimal composition, and therefore, the formed gel will be weaker and will not be effective^{35–38}. Therefore, it is essential to consider the adsorption values of the materials in the gelant for the optimal design of the operation^{30,38–43}.

In many research studies, the adsorption behavior of different polymers on sandstones and carbonate reservoirs has been investigated and tested in the laboratory^{33,35,42,44–46}. Also, the effect of impurities and other additives such as salt, nanoparticles, and surfactants on this process has been investigated^{22,47–50}. Most of the results show that the adsorption of polymers on the particles of sandstone or carbonate reservoirs is characterized by the Langmuir adsorption isotherm model^{51–57}. This fact shows that the adsorption of polymers on the surface of stones is in the form of a single layer, and they occupy the adsorption sites on their surfaces^{34,43,58–62}. Also, many researchers have reported that the increase in salinity or the presence of nanoparticles reduces the intensity of the adsorption of polymers, which also confirms the mechanism of the Langmuir model because, in this case, part of the adsorption sites related to rocks are occupied by other materials^{45,63,64}.

Also, the effect of temperature on the adsorption intensity of polymers has been investigated, and the results show that polymer adsorption increases with increasing temperature^{30,35,38,43,65}. Researchers consider this behavior related to reducing viscosity and increasing the mobility of polymer molecules^{66,67}. It should be noted that the effect of temperature on polymers is precisely the opposite of the behavior of surfactants. Surfactants, widely used materials in enhanced oil recovery, have been modeled significantly for their adsorption in different reservoirs^{32,68–71}. This adsorption modeling is not only instrumental in the field of experiment design, but it is also helpful in the surfactant selection process, and depending on the lithology of the reservoirs and the obtained adsorption models, the most suitable surfactant with less adsorption is selected^{45,60,72,73}.

The adsorption behavior and dynamic and static modeling of adsorption of different surfactants on rocks with different lithology, such as sandstone, carbonate, and clay, have been extensively studied and investigated^{31,40,74–76}. Today, large oil companies benefit from the data obtained by researchers when designing operations to enhance oil recovery^{77,78}. Also, significant work has been done to discuss the adsorption of polymers on the surfaces of various rocks because polymer injection is not only about the injection of the gel but is also used in fracturing fluid or solving viscous fingering problems^{79–81}. On the other hand, no special attention has been paid to modeling and investigating the adsorption behavior of crosslinkers in gelants, and this issue has not usually been studied and investigated. Urotropine is one of the crosslinkers used in the in-situ gel injection field, sometimes injected into sandstone reservoirs. Urotropine consists of 6 methyl groups and four amino groups, which have wide applications in various industries, including medicine, pharmaceuticals, and oil^{82–85}.

Sandstone reservoirs often have clay particles, which have a high adsorption capacity due to their lamellar structure and high specific surface and can strongly affect the gelant composition in areas far from the wellbore^{86,87}. There are different types of clay, one of the most common types of which is kaolinite. So far, no study has been done on the adsorption behavior and adsorption modeling of Urotropine on kaolinite. This process has been specially addressed in this research.

While significant research has focused on polymer and surfactant adsorption in enhanced oil recovery processes, the adsorption behavior of crosslinkers, particularly Urotropine, on reservoir rock components has received comparatively less attention. Urotropine is a widely utilized crosslinker in in-situ gel systems, crucial for modifying rheological properties and ensuring gel stability in heterogeneous porous media^{88–90}. Its interaction with reservoir minerals directly impacts gelant integrity and placement efficiency, yet comprehensive studies elucidating its adsorption mechanisms, especially on common clay minerals like kaolinite, are scarce. Kaolinite, a prominent aluminosilicate clay, is ubiquitous in sandstone reservoirs and possesses a high specific surface area and lamellar structure, making it a critical adsorbent. This research uniquely addresses this knowledge gap by providing a detailed investigation into the adsorption isotherms and thermodynamics of Urotropine on purified

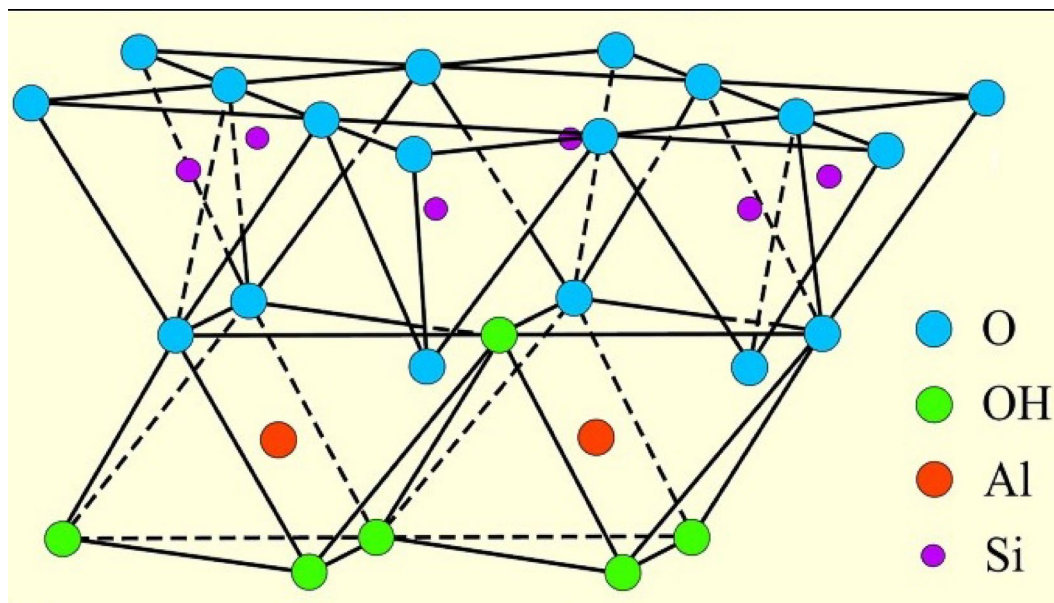


Fig. 1. Chemical structure and composition of kaolinite crystals.

Specification	Mass%
Kaolinite	97.48
Chloride	1.125
Sulphate	0.9
Heavy Metals	0.5

Table 1. XRD analysis results for kaolinite particles used in this study.

kaolinite particles, thereby offering fundamental insights into crosslinker-mineral interactions that are vital for robust gelant design and accurate predictive modeling of water shut-off treatments in mature oilfields.

In this research work, Urotropine adsorption values in solutions with different concentrations on very fine and pure kaolinite particles at 25 °C were done. The laboratory data obtained by widely used adsorption isotherm methods and models were fit, and the most suitable model was selected for this purpose. Then, by repeating the experiments at higher temperatures, the effect of temperature on this process was also investigated. Also, by thermodynamic modeling of adsorption behavior at different temperatures, process enthalpy changes, entropy changes, and Gibbs free energy were calculated, which show whether the process is spontaneous or forced. Since adsorption in porous media may not be the same as the results of batch experiments due to the complexities and presence of inaccessible areas, six kaolinite sandpacks were flooded with 10⁵ ppm Urotropine solution at different temperatures.

Materials and methods

Materials

Adsorbent (kaolinite)

In current research, kaolinite particles were used as adsorbents. Kaolinite is a type of clay that may be abundant in sandstone reservoirs. Usually, the phenomenon of fine migration is attributed to the presence of kaolinite particles. These particles are usually *aluminosilicate*; their overall composition is Al₂Si₂O₅(OH)₄. The structure of kaolinite crystals is usually layered, and the particle size of this mineral is tiny and smaller than 2 μm^{32,91–95}. These two features have caused kaolinite to have a high adsorption capacity. The chemical structure of kaolinite can be seen in Fig. 1.

The kaolinite used in this study, sourced from Pars Ore Company, boasts over 97% purity. Its XRD analysis results are presented in Table 1.

To prevent the integration of particles, grind them first and then use screen mesh No. 400 passed.

Adsorbate (Urotropine)

The organic compound Urotropine has the chemical formula C₆H₁₂N₄. Urotropine comprises six methylene units (–CH₂–) and four amino groups (–NH₂). The main application of Urotropine in the oil and gas industry is as a crosslinker in in-situ gel injection processes. After some time, this substance turns the polymer solution into a gel by dissolving it in the polymer solution and keeping it at the right temperature. This gel is usually used

in water shut-off processes, and depending on the need, it may be injected into oil production wells and water injection wells^{22,29,59,96–98}.

Urotropine used in this research was purchased from Merck with more than 99% purity. It should be noted that the solubility of this substance in water is very high, but it is usually used in concentrations of 0.5–4% by weight in the oil industry. With the aim of a more comprehensive study, solutions containing 0.01 wt% to 10% wt% (10^2 to 10^5 ppm) were studied in this research.

Experimental procedure

Preparation of aqueous solution

In this research, dozens of Urotropine solution samples were made in distilled water, with a concentration between 10^2 and 10^5 ppm. In this regard, the specified and measured amounts of Urotropine were added to one hundred milliliters of distilled water and mixed with a magnetic stirrer at 400 rpm. Due to the high solubility of this material in water, the prepared solution was seen as homogeneous and uniform after less than a minute, but to ensure more certainty, the mixing process was continued for 10 min.

These solutions, which had specific concentrations of Urotropine, were used to calibrate the UV device and validate its results. UV device was used to detect the concentration of solutions containing Urotropine. Its chemical structure is indicated in Fig. 2.

Since the accuracy and correctness of the information are very important in modeling the adsorption behavior of different substances, the device used is calibrated with high accuracy, and its measurement accuracy (error less than 0.1%) is ensured by measuring the concentration of specific solutions. Became.

Adsorption test as a batch experiment

The amount and intensity of Urotropine adsorption on kaolinite particles were measured and calculated according to the following procedure. This procedure has been recommended and suggested in various articles and books to measure the adsorption of surfactants on stone particles^{99–101}.

1. 100 mL of the initial solution with a specific concentration of Urotropine was made according to the principles mentioned in the previous section.
2. The amount of 20 g of powdered kaolinite was poured into each Urotropine solution and stirred for 24 h by a magnetic stirrer at 400 rpm until the adsorption process reached its maximum value.
3. The aqueous phase containing Urotropine adsorbent kaolinites for 30 min in a centrifuge machine with a dose of 6000 rpm was set. At this stage, all the kaolinite particles related to the device were collected at the end of the tube, and there were no kaolinite particles in the upper parts of the tube.

mL of the solution was removed from the top of the centrifuge tube, and its concentration was measured using a UV device. The UV device used in this step is MAPADA V-100 D.

5. Using the initial concentration, the concentration after the adsorption process and the mass of kaolinite were calculated based on Eq. 1.

$$q_e = 1000 \frac{(C_i - C_e)V_s}{m_k} \quad (1)$$

where C_i refers to the concentration of adsorbate in the initial condition, C_e is the concentration of the same material in the equilibrium state when the adsorption is done. V_s stands for the volume of solution, and m_k is the mass of kaolinite grains.

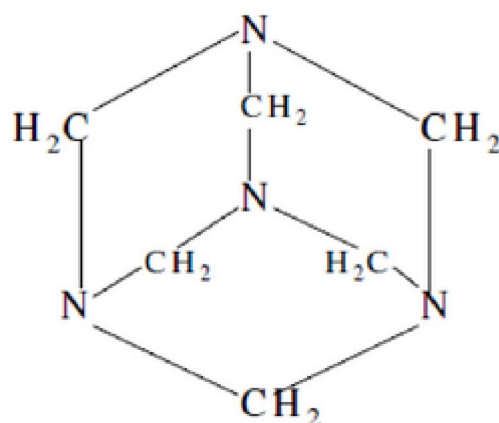


Fig. 2. Chemical structure of Urotropine.

Adsorption measurement in porous media

The laboratory procedure explained in the previous part is related to the batch experiment mode so that the solution's contact surface and adsorbent particles reach their maximum value. As a result, in such a test, the amount of adsorption will be higher than the actual state of the tank, which is a porous medium. The reason why researchers are interested in conducting batch experiments is the accuracy of the output models because the uncertainty parameters that exist in the porous medium do not occur in the batch experiment mode.

Nevertheless, evaluating the adsorption values of different solutions in porous environments is essential because the injected solutions are related to the porous environments of the rock in reservoirs and in the actual state. For this purpose, six sand-packs containing kaolinite particles were made and flooded with 10^5 ppm Urotropine solutions at different temperatures. The procedure for this test is as follows.

- 1 The sand-pack was made of kaolinite particles. For this purpose, a sleeve with an inner diameter of 1 inch and an outer diameter of 1.5 inches was chosen. Then, step by step, kaolinite particles were poured into it and pressed by the uniaxial device to complete the packing process. Then, on both sides of the sand-pack, two screen mesh No. 400 was glued to prevent kaolinite particles from coming out.
- 2 The prepared sand-packs were placed in the Vinci core flooding setup's core holder, and a confining pressure of 1000 psi was applied at the test temperature.
- 3 For 4 h, the system was tested at the temperature until all the components reached the mentioned temperature.
- 4 A solution of 10^5 ppm Urotropine was made to the size of 10 pore volume and poured into the accumulator.
- 5 10 times the volume of the holes were injected into the sandpack from the Urotropine solution. If possible, this test should be continued until the Urotropine concentration in the outlet fluid is the same as the injection fluid.
- 6 Calculating the amount of adsorption is calculated through Eq. 2.

$$q_e = \frac{V_o \cdot (10^5 - C_e)}{m_s} \quad (2)$$

where V_o is the volume of Urotropine solution in the outlet and m_s refers to the dry weight of the kaolinite sand-pack. Note the raw experimental data are available in the supplementary material.

Modeling method and data analysis

Adsorption isotherm models

Different isotherm models, including Langmuir, Freundlich, Temkin, and linear adsorption models, were used to analyze Urotropine adsorption data on kaolinite particles. The analysis was such that the obtained laboratory data were drawn in a graph where the X-axis was C_e and the Y-axis was q_e . Then, regression methods matched the mentioned models with the laboratory data in the best possible way. By drawing the studied models along with the laboratory data through statistical methods, the best model describing fluid behavior was selected, which was used for other steps. Brief explanations about the relationships and theories of these models are given in this section.

Langmuir isotherm model The primary assumption of this model is the uniformity of adsorption in the process. This model assumes that all adsorption sites are similar and independent at the adsorbent level. Therefore, the effectiveness of this model in predicting the adsorption of a type of chemical substance that is adsorbed as a single layer on the adsorption site of the adsorbent is appropriate. The primary relationship of this model is given in Eq. 3.

$$q_e = q_o \frac{K_L C_e}{1 + K_L C_e} \rightarrow \frac{q_e}{q_o} = \frac{K_L C_e}{1 + K_L C_e} \rightarrow \frac{1}{q_e} = \left(\frac{1}{K_L q_o} \right) \frac{1}{C_e} + \frac{1}{q_o} \quad (3)$$

In this equation, K_L is the Langmuir equilibrium constant (L/mg), and q_o refers to the adsorption capacity determined by the Langmuir isotherm model.

Due to its simplicity and capacity for accurate predictions, this model is commonly utilized in adsorption research¹⁰².

Temkin model In this model, it is assumed that the adsorption occurs in multilayers, and the adsorption energy decreases with the number of layers. This means that the adsorption energy for the third adsorbate layer on the adsorption site corresponding to the adsorbent is lower than that of the first layer. This model is non-linear, based on the interaction between adsorbate molecules with each other and with the adsorbent surface. It should be noted that most adsorption isotherms models are non-linear because the adsorption behavior is often non-linear. The general relationship of the Temkin model is written in Eq. 4.

$$q_e b = RT(\ln(K_T) + \ln(C_e)) \rightarrow q_e = \frac{RT}{b} \ln(K_T) + \frac{RT}{b} \ln(C_e) \quad (4)$$

where K_T refers to the Temkin equilibrium constant, b stands for the Temkin constant, T is the temperature at which adsorption occurs, and R denotes the global gas constant¹⁰³.

Freundlich model Like Temkin, this model assumes multi-layered adsorption behavior, with the difference that in the Freundlich model, it is assumed that the adsorbate surface is completely heterogeneous, and the adsorption process occurs heterogeneously. This model is also non-linear like the previous two models and is generally described by Eq. 5.

$$q_e = (K_f) (C_e)^{\frac{1}{n}} \rightarrow \ln(q_e) = \ln(K_f) + \frac{1}{n} \ln(C_e) \quad (5)$$

The Freundlich model includes K_f , a process constant related to adsorption capacity, and n , an exponent that shows the deviation from a linear isotherm. It's especially efficient for describing multi-layered and non-linear adsorption, providing insight into changes in adsorption behavior¹⁰⁴.

Linear model This model is a straightforward and low-accuracy method to describe the adsorption behavior of adsorbate on adsorbent surfaces. The accuracy of this method is more acceptable at low concentration when most adsorption sites are still empty. As the solution concentration increases, the performance accurateness of this model also decreases in forecasting the adsorption behavior performance. In general, Eq. 6, the equation of a straight line, describes the linear model.

$$q_e = KC_e + I \quad (6)$$

where K is the linear isotherm model constant and equals the slope, and I denotes to the intercept of the linear model¹⁰⁵.

Error analysis and model accuracy

The actual adsorption values were plotted with the values predicted by the models in a graph, and then the points predicted by the model were compared with the experimental values. This comparison can also be made visually by comparing the trends of the graphs and the amount. The values of the models can be close to the laboratory values, and different statistical analyses can be used in this regard. In this study, different models were evaluated using statistical studies. The models used are as follows.

ARE (Absolute Relative Error) ARE is used as a measure to evaluate the accuracy of models and compare them with actual values. This method is straightforward, understandable, and simultaneously practical, and the results obtained are reliable. Equation 7 calculates ARE values¹⁰⁶.

$$ARE = \frac{1}{n} \sum_{i=1}^n \left| \frac{q_{e,cal} - q_{e,lab}}{q_{e,lab}} \right|_i \quad (7)$$

ASE (Absolute Sum of Errors) This statistical indicator shows the total amount of errors. In this method, larger values are more effective, and in this research work, it can be claimed that the ASE method focuses more on the adsorption error of higher concentrations of Urotropine on kaolinite¹⁰⁷. This quantity is calculated from Eq. 8.

$$ASE = \frac{1}{n} \sum_{i=1}^n (q_{e,cal} - q_{e,lab})_i^2 \quad (8)$$

Correlation coefficient (R^2) R^2 statistically represents how much of the dependent variable's variation is accounted for by the independent variables within a regression model. The value of this statistical quantity is a thread to evaluate the effectiveness of predictive models. It should be noted that values close to 1 for this quantity indicate higher predictive model accuracy¹⁰⁸.

Thermodynamic modeling of the adsorption process

The effect of temperature on the adsorption of Urotropine on kaolinite was investigated through thermodynamic modeling. This powerful method aids in understanding the adsorption mechanism and in quantifying the energy changes that occur. From experimental adsorption data collected across a range of temperatures, essential thermodynamic parameters such as ΔH° , ΔS° , and ΔG° can be precisely determined¹⁰⁹.

Gibbs free energy deviations (ΔG°) calculation Equation 9 can be used to calculate the Gibbs free energy change for an adsorption process.

$$\Delta G^\circ = -RT \ln(K_D) \quad (9)$$

Equation 9 introduces K_D , the thermodynamic equilibrium constant, which is given in units of moles of water per mole of adsorbent. This constant is obtained by finding the intercept of a plot of q_e/C_e against q_e . R signifies the universal gas constant, and T is the experimental temperature measured in Kelvin. Subsequently, in accordance with the second law of thermodynamics, the value of ΔG° is calculated using Eq. 10.

$$\Delta G^\circ = \Delta H^\circ - T\Delta S^\circ \quad (10)$$

Here, ΔH° denotes the system's enthalpy change, and ΔS° represents the entropy change. A negative ΔG° value indicates a spontaneous process, whereas a positive value signifies a non-spontaneous one¹¹⁰. By integrating Eqs. 9 and 10, Eq. 11 is formed.

$$\ln(K_D) = -\frac{\Delta H^\circ}{RT} + \frac{\Delta S^\circ}{R} - 1.204 \quad (11)$$

In which 1.204 transfers the unit of K_D from mole_{water}/mole_{rock} to gr_{water}/gr_{rock}. Regarding Eq. 11, by plotting $\ln(K_D)$ versus $1/T$, ΔH° and ΔS° will be found:- slope $\times R$ and (intercept + 1.204) $\times R$ ¹¹¹.

Results and discussion

Adsorption behavior modeling

The adsorption test was made for solutions with different concentrations of Urotropine, which ranged from 10^2 to 10^5 ppm, and their adsorption values were measured on kaolinite particles at a temperature of 25 °C. The mentioned data are shown in Fig. 3. In this figure, the separate points are related to the results obtained in the laboratory, and the connected lines are related to the trend and prediction obtained from the behavior of Urotropine adsorption on kaolinite particles, which were obtained based on the same laboratory data.

As presented in Fig. 3, the Langmuir adsorption isotherm predicts the values and trends of adsorption with higher accuracy than other models. Nevertheless, it is essential to perform a statistical investigation and review the accuracy of the prediction of various methods. In Table 2, the obtained constants and equations for different models are written, as well as the statistical values of the prediction accuracy of each of them. All three statistical quantities express the high accuracy of the Langmuir model. This model estimates the adsorption capacity (q_0) of Urotropine on kaolinite particles to be 112 mg- Urotropine/g-kaolinite. Each gram of kaolinite in the batch experiment can adsorb about 0.112 g of Urotropine. This adsorption rate is relatively high and can challenge the composition of the injection gel in areas far from the well.

Regarding the Table 2 and the results of statistical analysis, Langmuir model has the lowest error and the highest correlation with the results obtained from the laboratory.

The robust fit of the Langmuir model ($R^2=0.992$, ARE=0.12%) over other isotherm models signifies a monolayer adsorption of Urotropine onto the kaolinite surface. This suggests that Urotropine molecules

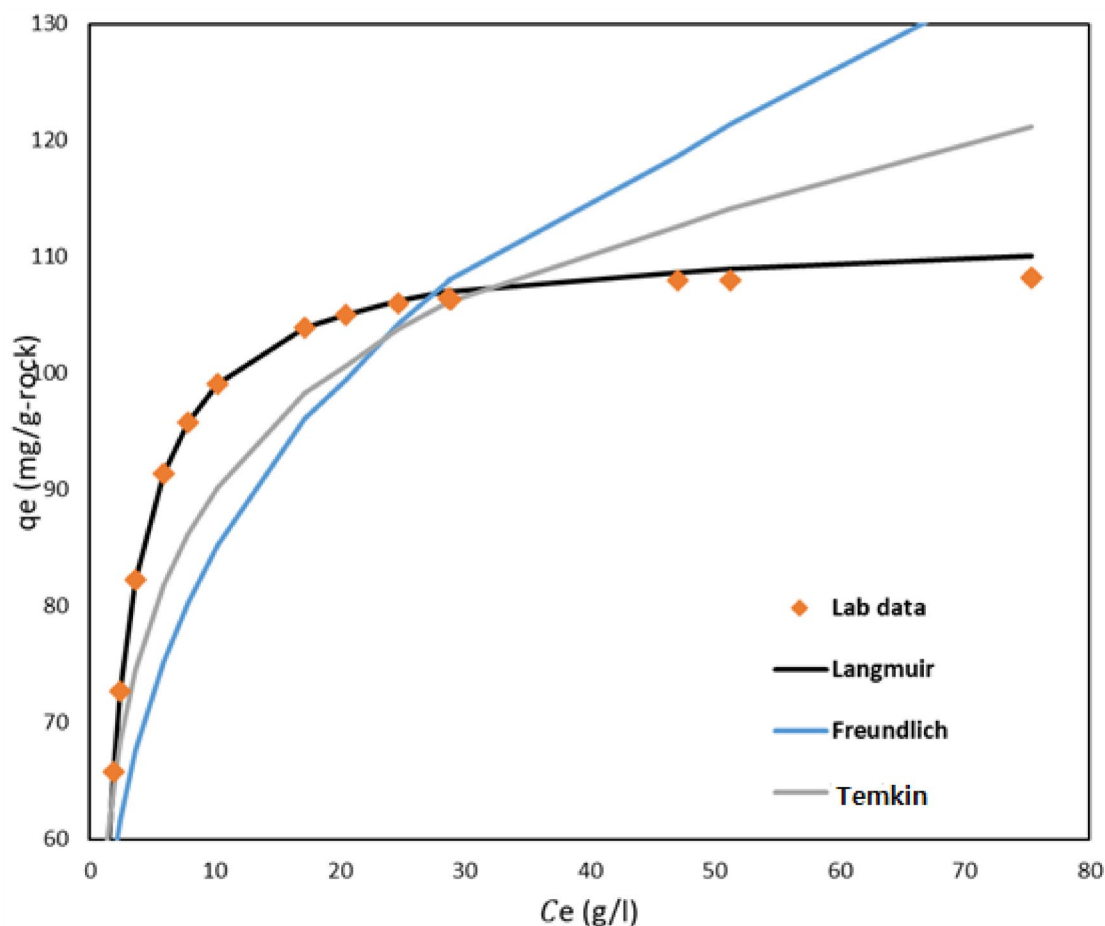


Fig. 3. Experimental adsorption data obtained for Urotropine on kaolinite particles and modeling results.

Model	Model constants	R2	ARE (%)	ASE (mg/g)
Langmuir	KL=0.74 L/mg	0.992	0.12	0.023
	qo = 112.1 mg/g			
Temkin	b = 15.4 J/mol	0.913	5.4	8.4
	KT= 34.4 L/mg			
Freundlich	Kf= 50.2 (mg/g)/(mg/L)^(1/n)	0.798	12.2	21.2
	n = 4.4			

Table 2. Results of experimental adsorption data and authentication of various models.

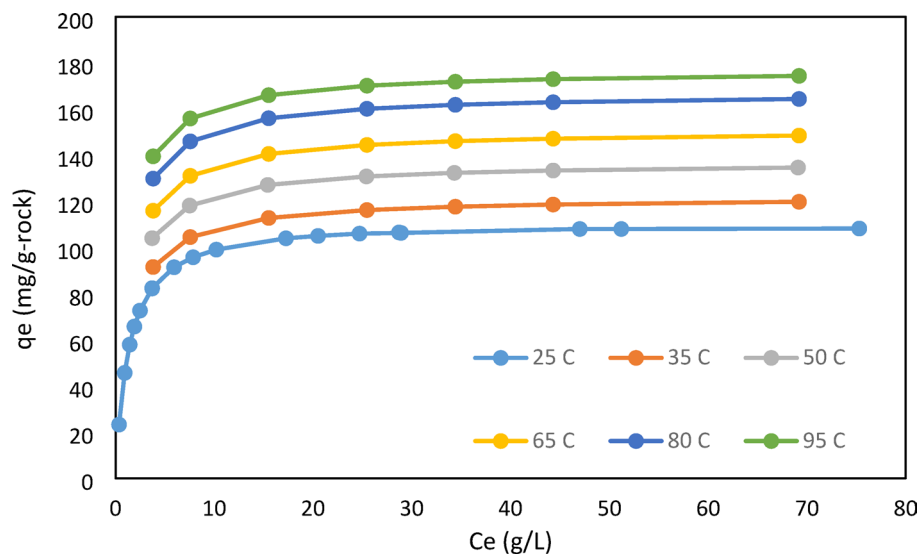


Fig. 4. Experimental adsorption obtained at different temperatures.

Temperature (°C)	25	35	50	65	80	95
K_L (L/mg)	0.755	0.79	0.83	0.87	0.92	0.98
q_o (mg/g)	112.2	122	132	151	167	177
ARE (%)	0.12	0.1	0.09	0.13	0.15	0.11

Table 3. Langmuir model constants obtained from testing in various temperatures.

primarily occupy a finite number of active sites on the kaolinite, with no significant interaction among adsorbed molecules. The determined maximum monolayer adsorption capacity (q_o) of 112.1 mg/g-kaolinite at 25 °C is notably high, implying a strong affinity between Urotropine and the kaolinite surface. This high adsorption capacity is critical from a practical standpoint, as it indicates a substantial loss of crosslinker concentration from the gelant solution before it reaches the target zone in the reservoir. Such a reduction in Urotropine concentration can compromise the integrity and strength of the formed gel, potentially leading to suboptimal water shut-off performance. The adsorption mechanism is likely driven by hydrogen bonding among the amine groups of Urotropine and the hydroxyl groups present on the kaolinite surface, as well as potential electrostatic interactions given the slightly negative charge of kaolinite surfaces in aqueous solutions. The uniform nature of adsorption sites, as implied by the Langmuir model, aligns with the well-defined crystal structure of kaolinite.

Temperature effect on adsorption behavior

The experiment measuring the adsorption values of Urotropine solutions on kaolinite particles at higher temperatures, including 35, 50, 65, 80, and 95 °C, was also repeated. The laboratory data obtained from this step is revealed in Fig. 4. Based on this figure, increasing the temperature increases the adsorption values. This trend signifies that the process is endothermic. Therefore, the enthalpy of the Urotropine adsorption process on quartz is expected to be a negative number, which will be calculated with higher accuracy in the following sections.

Based on the data in the above figure, the Langmuir model was also utilized to the results obtained from the laboratory at higher temperatures, and the statistical analyses showed a perfect and acceptable adaptation of this model. The constants related to the Langmuir model and the results of their statistical study are given in Table 3.

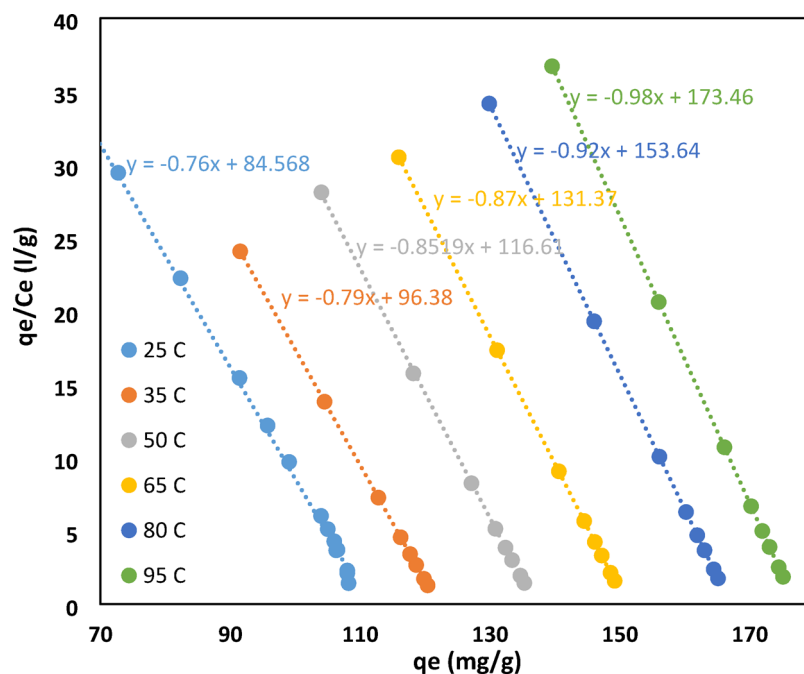


Fig. 5. Q_e/c_e plot versus q_e in different temperatures used for thermodynamic study.

T (°C)	1/T (1/K)	K _d (L/g)	Ln (K _d)	ΔG° (J/mole)
25	0.0033557	84.00	4.431	-13,994.3
35	0.0032468	96.38	4.568	-14,777.8
50	0.0030960	116.61	4.759	-15,953.05
65	0.0029586	131.37	4.878	-17,128.3
80	0.0028329	153.64	5.035	-18,303.55
95	0.0027174	173.46	5.156	-19,478.8
Slope	-1125.1	Intercept	8.22	

Table 4. Thermodynamic results obtained from modeling of adsorption behavior in various temperatures.

Based on this table, both the adsorption capability and the equilibrium constant increase with increasing temperature, both of which show that this process is endothermic. The adsorption capacity, which was 112 mg/g-kaolinite at 25 °C, reaches 182 at 95 °C, and the equilibrium constant of the process increases from 0.73 to 0.98.

Thermodynamic modeling

This part modeled and investigated the thermodynamic behavior of the Urotropine adsorption process on kaolinite particles. In this regard, the first q_e/c_e was drawn in terms of q_e for the adsorption behavior measured at different temperatures. Based on the thermodynamic modeling method explained in the previous section, the interception of these lines indicates K_d . This parameter is critical and valuable in thermodynamic study. Figure 5 shows the diagram related to this part, and the gravity equations are also evident.

Based on the above figure, the K_d values obtained for different temperatures were obtained and are presented in Table 4. Different values of K_d at different temperatures indicate that this parameter has a direct relationship with temperature. Then, in the next step, by plotting $\ln(K_d)$ VS. $1/T$, the values of entropy and enthalpy changes can be calculated using Eq. 11. Based on this, the process enthalpy value of 9354 J/mole was obtained. The positive value of this quantity for the Urotropine process on kaolinite shows that this is an utterly endothermic process, and higher temperatures help increase the balance of the process to the right. Based on the principles of regression and performing calculations, the amount of entropy changes was also obtained as 78.35 J/mole.K. According to Eq. 11, which calculates the amount of Gibbs free energy changes at a specific temperature, it can be found that this value is for the adsorption process of Urotropine on kaolinite particles at temperatures higher than -153 °C, which is a negative number. Therefore, it is an entirely spontaneous process.

The positive enthalpy change ($\Delta H^\circ = 9354$ J/mole) definitively confirms the endothermic nature of Urotropine adsorption on kaolinite. This is a crucial finding, indicating that the adsorption procedure is favored by increasing temperature, as observed in the experimental data where adsorption capacity systematically increased from 112 mg/g @ 25 °C to 177 mg/g @ 95 °C. This endothermic behavior contrasts with many typical physical adsorption processes, which are often exothermic. The positive entropy change ($\Delta S^\circ = 78.35$ J/mole.K) further suggests an

No	T (°C)	Length (cm)	Diameter (cm)	Dry weight (gr)	Porosity (vol%)	Outlet volume (mL)	Outlet urotropine concentration (ppm)	qe (mg-urotropine /gr-rock)
1	25	10	2.54	102	22.5	420	83,943	66.12
2	35	10	2.54	101.2	23.1	432	81,234	80.11
3	50	10	2.54	99.4	24.5	440	80,212	87.59
4	65	10	2.54	100.5	23.7	460	78,234	99.63
5	80	10	2.54	100.9	23.4	459	77,023	104.52
6	95	10	2.54	101.2	23.1	465	75,421	112.94

Table 5. Flooding sand-pack specifications and results obtained from porous media adsorption experiment.

increase in the randomness or disorder at the solid–liquid interface during the adsorption. This can be ascribed to the displacement of water molecules from the kaolinite surface by Urotropine molecules or increased conformational freedom of the adsorbed Urotropine at higher temperatures. The consistently negative values of Gibbs free energy (ΔG°) across all studied temperatures, ranging from $-13,994.3$ J/mole at 25°C to $-19,478.8$ J/mole at 95°C , unequivocally demonstrate the spontaneous nature of Urotropine adsorption on kaolinite. The increasing negativity of ΔG° with temperature further reinforces that higher temperatures enhance the spontaneity and favorability of the adsorption process. In practical terms, this implies that in warmer reservoir environments, a greater amount of Urotropine will be adsorbed onto the kaolinite, necessitating adjustments in gelant formulation to ensure sufficient crosslinker reaches the target zone for effective gelation.

Table 4 calculates Kd values and Gibbs free energy changes for different temperatures, confirming the explanations presented in this section.

The above table confirms the spontaneity and endothermicity of the Urotropine adsorption on kaolinite particles. This upsurge in adsorption capacity and process balance can be interrelated to the increased movement and speed of Urotropine molecules. Urotropine particles communicate with kaolinite surfaces based on hydrogen bonding and are adsorbed on it, increasing the process's speed and viscosity reduction.

Adsorption performance in porous media

At this section, six kaolinite sand-packs were made using the previously mentioned method. A large quantity of 10^5 ppm Urotropine solution was then made. This solution was continued at different temperatures, including 25°C , 35°C , 50°C , 65°C , 80°C , and 95°C , into the sand-packs until the concentration of Urotropine in the output fluid reached the initial value. The results of this part and the general features of sand-packs are given in Table 5.

The above table, like the results from the previous sections, designates that this procedure is endothermic, and the adsorption capacity increases by temperature. The adsorption capacity was 66 mg/g-rock at 25°C , while this quantity was associated with an increase of 112 at 95°C .

Another essential thing evident in this table is the lower adsorption rate in the injection into the porous media compared to the batch tests. In the porous medium, there are complications in the direction of the solution flow, and part of the holes and part of the surface of the particles are accessible for the injection solution. In the batch experiment, the entire surface of the kaolinite particles was exposed to the Urotropine solution, and therefore, the adsorption process happened more intensively and quickly.

The complexity of the porous medium and the inaccessibility of some particles for injection solutions caused the adsorption capacity to decrease from 112 to 66 at 25°C , and this decrease was from 182 to 114 at 95°C .

Conclusion

In this research, the adsorption performance of Urotropine was tested at various temperatures and conditions, and this adsorption behavior was compared with different models. In the next step, thermodynamic modeling of the behavior of this adsorption process was also done. Finally, a solution containing 10^5 ppm of Urotropine was injected into kaolinite sand-packs to check the adsorption values of this substance on kaolinite in the porous medium. In general, the results obtained are as follows:

- 1 The Langmuir isotherm model is the best model that describes the adsorption behavior of Urotropine solution at different temperatures on kaolinite particles. Adsorption capacity reached 112 mg/g-rock at a temperature of 25°C , which is a relatively high figure, and it is necessary to consider this material as a polymer crosslinker in industrial designs when injecting it.
- 2 With increasing temperature, the intensity and capacity of this process increased, which shows that this adsorption process is endothermic, and its enthalpy is estimated to be positive. In addition to constant adsorption capacity, the equilibrium of the process also increased with increasing temperature.
- 3 Thermodynamic modeling of the laboratory data showed that the enthalpy of the progression is 9354 J/mole, and its entropy changes are 73.85 J/mole.K. In fact, at temperatures higher than -153°C , the Gibbs free energy changes were negative and spontaneous, indicating this endothermic process.
- 4 In the last step, Urotropine solution with a concentration of 10^5 ppm was injected into kaolinite sand-packs at various temperatures. These results, like the previous part, showed the endothermal nature of the procedure and the increase in the adsorption capacity of Urotropine on kaolinite particles with increasing temperature. It was also found that the adsorption capacity in the porous-media was lower than the batch tests, which is related to the complication of the porous-media and the inaccessibility of some of the particles.

In general, this thermodynamic modeling investigates the adsorption performance of Urotropine. This substance is a strong crosslinker in the in-situ gel injection operation. The results of this test show this substance's high adsorption rate on clay particles. Therefore, it is essential to pay attention to this point in the operation design to prevent its failure and failure.

Data availability

Data is available in the supplementary file.

Received: 21 November 2024; Accepted: 5 September 2025

Published online: 08 October 2025

References

- Dong, T. et al. Quartz types and origins in the paleozoic Wufeng-Longmaxi Formations, Eastern Sichuan Basin, China: Implications for porosity preservation in shale reservoirs. *Mar. Pet. Geol.* **106**, 62–73 (2019).
- Shi, H. et al. Sources of quartz grains influencing quartz cementation and reservoir quality in ultra-deeply buried sandstones in Keshen-2 gas field, north-west China. *Mar. Pet. Geol.* **98**, 185–198 (2018).
- Belhaj, A. F. et al. The effect of surfactant concentration, salinity, temperature, and pH on surfactant adsorption for chemical enhanced oil recovery: A review. *J. Petrol. Explor. Prod. Technol.* **10**(1), 125–137 (2020).
- Saez, M. et al. *Improving Volumetric Efficiency in an Unconsolidated Sandstone Reservoir with Sequential Injection of Polymer Gels, in SPE Improved Oil Recovery Symposium*. pp. SPE-150492-MS (2012).
- Garcia, D. C. S., Wang, K. & Figueiredo, R. B. The influences of quartz content and water-to-binder ratio on the microstructure and hardness of autoclaved Portland cement pastes. *Cement Concr. Compos.* **91**, 138–147 (2018).
- Al-Shajalee, F. et al. A multiscale investigation of cross-linked polymer gel injection in sandstone gas reservoirs: Implications for water shutoff treatment. *Energy Fuels* **34**(11), 14046–14057 (2020).
- Goudarzi, A. et al. A laboratory and simulation study of preformed particle gels for water conformance control. *Fuel* **140**, 502–513 (2015).
- Sengupta, B., Sharma, V. P. & Udayabhanu, G. In-situ gelation studies of an eco-friendly cross-linked polymer system for water shut-off at high temperatures. *Energy Sources Part A Recov. Util Environ Effects* **36**(13), 1445–1467 (2014).
- Abedi Lenji, M. et al. Gelation Time of Hexamethylenetetramine Polymer Gels Used in Water Shutoff Treatment. *J. Pet. Sci. Technol.* **2**(2), 3–11 (2012).
- Hazbeh, O. et al. Hybrid computing models to predict oil formation volume factor using multilayer perceptron algorithm. *J. Petrol. Min. Eng.* **23**(1), 17–30 (2021).
- Rajabi, M., Ghorbani, H. & Khezerloo-ye Aghdam, S. Prediction of shear wave velocity by extreme learning machine technique from well log data. *J. Petrol. Geomech.* **4**(3), 35–49 (2013).
- Dicharry, R. M., Perryman, T. L. & Ronquille, J. D. Evaluation and Design of a CO₂ Miscible Flood Project-SACROC Unit Kelly-Snyder Field. *J. Petrol. Technol.* **25**(11), 1309–1318 (1973).
- Al-Attar, H. H. et al. *Low Salinity Flooding in a Selected Carbonate Reservoir: Experimental Approach*, In: *EAGE Annual Conference & Exhibition incorporating SPE Europec*. pp. SPE-164788-MS (2013).
- Sharifi, O. et al. Laboratory study of the application of a novel bio-based polymer to synthesize Aphron drilling fluids. *J. Pet. Sci. Technol.* **12**(2), 42–50 (2022).
- Rajabi, M., Ghorbani, H. & Khezerloo-ye Aghdam, S. Sensitivity analysis of effective factors for estimating formation pore pressure using a new method: The LSSVM-PSO algorithm. *J. Petrol. Geomech.* **4**(3), 96–113 (2022).
- Adu, E., Zhang, Y. & Liu, D. Current situation of carbon dioxide capture, storage, and enhanced oil recovery in the oil and gas industry. *The Canadian Journal of Chemical Engineering* **97**(5), 1048–1076 (2019).
- Bachu, S. and J. Shaw, *Evaluation of the CO₂ Sequestration Capacity in Alberta's Oil and Gas Reservoirs at Depletion and the Effect of Underlying Aquifers*. Journal of Canadian Petroleum Technology, **42**(09) (2003).
- Leng, J., Wei, M. & Bai, B. Review of transport mechanisms and numerical simulation studies of preformed particle gel for conformance control. *J. Petrol. Sci. Eng.* **206**, 109051 (2021).
- Rohem Peçanha, E. et al. Interaction forces between colloidal starch and quartz and hematite particles in mineral flotation. *Colloids Surf., A* **562**, 79–85 (2019).
- Al-Muntasheri, G. A., Nasr-El-Din, H. A. & Hussein, I. A. A rheological investigation of a high temperature organic gel used for water shut-off treatments. *J. Petrol. Sci. Eng.* **59**(1), 73–83 (2007).
- Al-Muntasheri, G. A. et al. Viscoelastic properties of a high temperature cross-linked water shut-off polymeric gel. *J. Petrol. Sci. Eng.* **55**(1), 56–66 (2007).
- Fang, J. et al. *Experimental research of hydroquinone (HQ)/hexamethylene tetramine (HMTA) gel for water plugging treatments in high-temperature and high-salinity reservoirs*. Journal of Applied Polymer Science, **134**(1) (2017).
- Grattoni, C. A., Jing, X. D. and Zimmerman, R. W. *Disproportionate Permeability Reduction when a Silicate Gel is Formed In-Situ to Control Water Production*, in *SPE Latin American and Caribbean Petroleum Engineering Conference*. pp. SPE-69534-MS (2001).
- Shi, C. et al. Insight into a bentonite-based hydrogel for the conservation of sandstone-based cultural heritage: In situ formation, reinforcement mechanism, and high-durability evaluation. *ACS Appl. Mater. Interfaces* **14**(46), 52459–52466 (2022).
- Zhong, H. et al. Inhibiting shale hydration and dispersion with amine-terminated polyamidoamine dendrimers. *J. Nat. Gas Sci. Eng.* **28**, 52–60 (2016).
- Zareie, C. et al. Network-gel strength relationship and performance improvement of polyacrylamide hydrogel using nano-silica; with regards to application in oil wells conditions. *J. Mol. Liq.* **278**, 512–520 (2019).
- Yang, Q. et al. The experimental study of silica nanoparticles strengthened polymer gel system. *J. Dispersion Sci. Technol.* **42**(2), 298–305 (2021).
- Shehbaz, S. M. & Bera, A. Effects of nanoparticles, polymer and accelerator concentrations, and salinity on gelation behavior of polymer gel systems for water shut-off jobs in oil reservoirs. *Petrol. Res.* **8**(2), 234–243 (2023).
- Jesuvathy Sornalatha, D. & Murugakoothan, P. Characterization of hexagonal ZnO nanostructures prepared by hexamethylenetetramine (HMTA) assisted wet chemical method. *Mater. Lett.* **124**, 219–222 (2014).
- Tongwa, P., Nygaard, R. & Bai, B. Evaluation of a nanocomposite hydrogel for water shut-off in enhanced oil recovery applications: Design, synthesis, and characterization. *J. Appl. Polym. Sci.* **128**(1), 787–794 (2013).
- Rajae, S. et al. Nanocomposite hydrogels adsorption: Experimental investigation and performance on sandstone core. *J. Petrol. Sci. Eng.* **159**, 934–941 (2017).
- Aghdam, S.K.-Y., Kazemi, A. & Ahmadi, M. Studying the effect of various surfactants on the possibility and intensity of fine migration during low-salinity water flooding in clay-rich sandstones. *Results Eng.* **18**, 101149 (2023).
- Rajae, S. et al. The adsorption of polyacrylamide nanocomposite hydrogels on sandstone. *J. Oil Gas Petrochem. Technol.* **2**, 1–13 (2015).

34. Aljeboree, A. M. et al. Synthesis of a new nanocomposite with the core TiO₂/hydrogel: Brilliant green dye adsorption, isotherms, kinetics, and DFT studies. *J. Ind. Eng. Chem.* **109**, 475–485 (2022).
35. Rajabi, M. S., Moradi, R. & Andrade, L. O. Chemically crosslinked polyvinyl alcohol for water shut-off and conformance control treatments during oil production: The effect of silica nanoparticles. *J. Appl. Polym. Sci.* **140**(4), e53382 (2023).
36. Khamees, T. K. & Flori, R. E. A comprehensive evaluation of the parameters that affect the performance of in-situ gelation system. *Fuel* **225**, 140–160 (2018).
37. Hamza, A. et al. Impact of aluminium acetate particles size on the gelation kinetics of polyacrylamide-based gels: Rheological and molecular simulation study. *Can. J. Chem. Eng.* **100**(6), 1169–1177 (2022).
38. Appel, E. A. et al. Self-assembled hydrogels utilizing polymer–nanoparticle interactions. *Nat. Commun.* **6**(1), 6295 (2015).
39. Kalam, S. et al. A review on surfactant retention on rocks: mechanisms, measurements, and influencing factors. *Fuel* **293**, 120459 (2021).
40. Ahmadi, M. A. & Shadizadeh, S. R. Experimental investigation of a natural surfactant adsorption on shale-sandstone reservoir rocks: Static and dynamic conditions. *Fuel* **159**, 15–26 (2015).
41. Iqbal, M. et al. High temperature stability and low adsorption of sub-100nm magnetite nanoparticles grafted with sulfonated copolymers on Berea sandstone in high salinity brine. *Colloids Surf., A* **520**, 257–267 (2017).
42. Yang, X. et al. Molecular dynamics simulations to study the adsorption damage of modified polyacrylamide in sandstone pores. *J. Mol. Liq.* **397**, 124096 (2024).
43. Naushad, M., Ahamad, T. & Al-Sheetan, K. M. Development of a polymeric nanocomposite as a high performance adsorbent for Pb(II) removal from water medium: Equilibrium, kinetic and antimicrobial activity. *J. Hazard. Mater.* **407**, 124816 (2021).
44. Wang, X. et al. Acetamide-modified hyper-cross-linked resin: Synthesis, characterization, and adsorption performance to phenol from aqueous solution. *J. Appl. Polymer Sci.* **132**(10), 41597 (2015).
45. Saxena, N. et al. Bio-based surfactant for enhanced oil recovery: Interfacial properties, emulsification and rock-fluid interactions. *J. Petrol. Sci. Eng.* **176**, 299–311 (2019).
46. Zhou, Z. J., Gunter, W. O. and Jonasson, R. G. *Controlling formation damage using clay stabilizers: A review*, In: *Annual Technical Meeting*. pp. PETSOC–95–71 (1995).
47. Jia, H. et al. Evaluation of polyacrylamide gels with accelerator ammonium salts for water shutoff in ultralow temperature reservoirs: Gelation performance and application recommendations. *Petroleum* **2**(1), 90–97 (2016).
48. Fathima, A. et al. Polymer nanocomposites for water shutoff application- A review. *Mater. Res. Express* **6**(3), 032001 (2019).
49. Bol, G. M. *The Effect of Various Polymers and Salts on Borehole and Cutting Stability in Water-Base Shale Drilling Fluids*, in *IADC/SPE Drilling Conference*. pp. SPE–14802–MS (1986).
50. Mercado, R., Martinez, R. & Rondón, M. Rheological demonstration of micellization changes of internal olefin sulfonate and alcohol alkoxy sulfate commercial surfactants upon interactions with inorganic salts. *Results Eng* **17**, 100792 (2023).
51. Moslemizadeh, A. et al. Assessment of swelling inhibitive effect of CTAB adsorption on montmorillonite in aqueous phase. *Appl. Clay Sci.* **127–128**, 111–122 (2016).
52. Aghdam, S. K.-Y. et al. *Thermodynamic Modeling of Saponin Adsorption Behavior on Sandstone Rocks: An Experimental Study*. Arabian Journal for Science and Engineering, (2022).
53. Craik, A. D. D. & Leibovich, S. A rational model for Langmuir circulations. *J. Fluid Mech.* **73**(3), 401–426 (1976).
54. Marczewski, A. W. Analysis of kinetic Langmuir model. Part I: Integrated kinetic langmuir equation (IKL): A new complete analytical solution of the langmuir rate equation. *Langmuir* **26**(19), 15229–15238 (2010).
55. Belton, G. R. Langmuir adsorption, the Gibbs adsorption isotherm, and interfacial kinetics in liquid metal systems. *Metall. Trans. B* **7**(1), 35–42 (1976).
56. Alafnan, S. et al. Langmuir adsorption isotherm in unconventional resources: Applicability and limitations. *J. Petrol. Sci. Eng.* **207**, 109172 (2021).
57. Guo, X. & Wang, J. Comparison of linearization methods for modeling the Langmuir adsorption isotherm. *J. Mol. Liq.* **296**, 111850 (2019).
58. Saha, R., Uppaluri, R. V. S. & Tiwari, P. Effect of mineralogy on the adsorption characteristics of surfactant–Reservoir rock system. *Colloids Surf., A* **531**, 121–132 (2017).
59. McPeak, K. M. et al. Chemical bath deposition of ZnO nanowires at near-neutral pH conditions without hexamethylenetetramine (HMTA): Understanding the role of HMTA in ZnO nanowire growth. *Langmuir* **27**(7), 3672–3677 (2011).
60. Aghdam, S.K.-Y. et al. Thermodynamic modeling of saponin adsorption behavior on sandstone rocks: An experimental study. *Arab. J. Sci. Eng.* **48**(7), 9461–9476 (2023).
61. Ramírez-Arias, A. M., Moreno-Piraján, J. C. & Giraldo, L. Adsorption of Triton X-100 in aqueous solution on activated carbon obtained from waste tires for wastewater decontamination. *Adsorption* **26**(2), 303–316 (2020).
62. Ahmad, R. & Mirza, A. Heavy metal remediation by Dextrin-oxalic acid/Cetyltrimethyl ammonium bromide (CTAB) – Montmorillonite (MMT) nanocomposite. *Groundw. Sustain. Dev.* **4**, 57–65 (2017).
63. Saxena, N., Kumar, A. & Mandal, A. Adsorption analysis of natural anionic surfactant for enhanced oil recovery: The role of mineralogy, salinity, alkalinity and nanoparticles. *J. Petrol. Sci. Eng.* **173**, 1264–1283 (2019).
64. Yeung, A., Dabros, T. & Masliyah, J. Dissipative Interfaces and Departures from the Young–Laplace Equation. *Langmuir* **13**(24), 6597–6606 (1997).
65. Sedev, R. & Exerowa, D. DLVO and non-DLVO surface forces in foam films from amphiphilic block copolymers. *Adv. Coll. Interface. Sci.* **83**(1), 111–136 (1999).
66. Venkatakrishnan, A. & Kuppa, V. K. Polymer adsorption on rough surfaces. *Curr. Opin. Chem. Eng.* **19**, 170–177 (2018).
67. O’Shea, J.-P., Qiao, G. G. & Franks, G. V. Solid–liquid separations with a temperature-responsive polymeric flocculant: Effect of temperature and molecular weight on polymer adsorption and deposition. *J. Colloid Interface Sci.* **348**(1), 9–23 (2010).
68. Shimabayashi, S. et al., Adsorption of Nonionic Surfactants, Triton X and Triton N, on Hydroxyapatite after Surface Modification with Sodium Dodecyl Sulfate in an Aqueous Phase*) This study was supported by Grant-in-Aid for Scientific Research (C)-(2) #11672143(1999–2000) of The Ministry of Education, Science, Sports and Culture, Japan, in *Studies in Surface Science and Catalysis*, Y. Iwasawa, N. Oyama, and H. Kunieda, Editors. Elsevier. pp. 125–128 (2001).
69. Khezloo-ye Aghdam, S., Kazemi, A. & Ahmadi, M. Studying the effect of surfactant assisted low-salinity water flooding on clay-rich sandstones. *Petroleum* **10**(2), 306–318 (2024).
70. Kalam, S. et al. Surfactant adsorption isotherms: A review. *ACS Omega* **6**(48), 32342–32348 (2021).
71. Kalam, S. et al. Adsorption mechanisms of a novel cationic gemini surfactant onto different rocks. *Energy Fuels* **36**(11), 5737–5748 (2022).
72. Ishiguro, M. & Koopal, L. K. Surfactant adsorption to soil components and soils. *Adv. Coll. Interface. Sci.* **231**, 59–102 (2016).
73. Becraft, K. A. & Richmond, G. L. Surfactant adsorption at the salt/water interface: comparing the conformation and interfacial water structure for selected surfactants. *J. Phys. Chem. B* **109**(11), 5108–5117 (2005).
74. Tang, G.-Q. & Morrow, N. R. Influence of brine composition and fines migration on crude oil/brine/rock interactions and oil recovery. *J. Petrol. Sci. Eng.* **24**(2), 99–111 (1999).
75. Hamza, A. et al. Impact of clays on CO₂ adsorption and enhanced gas recovery in sandstone reservoirs. *Int. J. Greenhouse Gas Control* **106**, 103286 (2021).
76. Barati-Harooni, A. et al. Experimental and modeling studies on adsorption of a nonionic surfactant on sandstone minerals in enhanced oil recovery process with surfactant flooding. *J. Mol. Liq.* **220**, 1022–1032 (2016).

77. Fu, X. et al. Quantitative synergistic adsorption affinity of Ca (II) and sodium oleate to predict the surface reactivity of hematite and quartz. *Sep. Purif. Technol.* **360**, 131196 (2025).
78. Yu, H. et al. Modeling thermal-induced wellhead growth through the lifecycle of a well. *Geoenergy Sci. Eng.* **241**, 213098 (2024).
79. Kargozarfard, Z., Riazi, M. & Ayatollahi, S. Viscous fingering and its effect on areal sweep efficiency during waterflooding: An experimental study. *Pet. Sci.* **16**(1), 105–116 (2019).
80. Yadali Jamaloei, B., Babolmorad, R. & Kharrat, R. Correlations of viscous fingering in heavy oil waterflooding. *Fuel* **179**, 97–102 (2016).
81. Talebian, S. H. et al. *Foam assisted CO₂-EOR; Concepts, Challenges and Applications*. In: *SPE Enhanced Oil Recovery Conference* (2013).
82. Feng, G. et al. Non-solvent displacement nonaqueous precipitation fabrication of novel foldable HAp ceramic paper without fiber and its performance. *Ceram. Int.* **50**(17), 29819–29830 (2024).
83. Feng, G. et al. Effect of oxygen donor alcohol on nonaqueous precipitation synthesis of alumina powders. *Ceram. Int.* **45**(1), 354–360 (2019).
84. Xu, J. et al. Study on fuel injection stability improvement in marine low-speed dual-fuel engines. *Appl. Therm. Eng.* **253**, 123729 (2024).
85. Zhang, Q. et al. Low temperature synthesis of ultrafine Al₂TiO₅ powders by hydrolytic sol-gel method. *Mater. Sci. Forum* **848**, 324 (2016).
86. Feng, G. et al. Group replacement–rearrangement-triggered linear-assembly nonaqueous precipitation synthesis of hydroxyapatite fibers. *ACS Biomater. Sci. Eng.* **9**(8), 4597–4606 (2023).
87. Li, Y. Y., Zhao, X. W. and Zhang, H. H. *Out-of-core solver based DDM for solving large airborne array*. Applied Computational Electromagnetics Society Journal (ACES), pp. 509–515 (2016).
88. Feng, G. et al. Novel facile nonaqueous precipitation in-situ synthesis of mullite whisker skeleton porous materials. *Ceram. Int.* **44**(18), 22904–22910 (2018).
89. Feng, G. et al. A novel green nonaqueous sol-gel process for preparation of partially stabilized zirconia nanopowder. *Process. Appl. Ceram.* **11**(3), 220–224 (2017).
90. Feng, G. et al. Synthesis and characterization of dense core-shell particles prepared by non-solvent displacement nonaqueous precipitation method taking C@ZrSiO₄ black pigment preparation as the case. *Colloid Interface Sci. Commun.* **57**, 100748 (2023).
91. Khezerloo-ye Aghdam, S., Kazemi, A. & Ahmadi, M. Theoretical and experimental study of fine migration during low-salinity water flooding: effect of brine composition on interparticle forces. *SPE Reserv. Eval. Eng.* **26**(02), 228–243 (2023).
92. Kazemi, A., Khezerloo-ye Aghdam, S. & Ahmadi, M. Theoretical and experimental investigation of the impact of oil functional groups on the performance of smart water in clay-rich sandstones. *Sci. Rep.* **14**(1), 20172 (2024).
93. Aghdam, S.K.-Y., Kazemi, A., and Ahmadi M. *Theoretical and Experimental Study of Fine Migration During Low-Salinity Water Flooding: Effect of Brine Composition on Interparticle Forces*. SPE Reservoir Evaluation & Engineering, pp. 1–16 (2022).
94. Rosenbrand, E. et al. Different effects of temperature and salinity on permeability reduction by fines migration in Berea sandstone. *Geothermics* **53**, 225–235 (2015).
95. Weber, C. & Kaufhold, S. Hamaker functions for kaolinite and montmorillonite. *Colloid Interface Sci. Commun.* **43**, 100442 (2021).
96. Liu, Y. et al. New insights into the hydroquinone (HQ)–hexamethylenetetramine (HMTA) gel system for water shut-off treatment in high temperature reservoirs. *J. Ind. Eng. Chem.* **35**, 20–28 (2016).
97. Strano, V. et al. Double role of HMTA in ZnO nanorods grown by chemical bath deposition. *J. Phys. Chem. C* **118**(48), 28189–28195 (2014).
98. Ahmadi, R. et al. Anthracite based activated carbon impregnated with HMTA as an effectiveness adsorbent could significantly uptake gasoline vapors. *Ecotoxicol. Environ. Saf.* **254**, 114698 (2023).
99. Feng, G. et al. Non-solvent displacement nonaqueous precipitation method for core-shell materials preparation: Synthesis of C@ZrSiO₄ black pigment. *Ceram. Int.* **49**(23), 38148–38156 (2023).
100. Feng, G. et al. Nonaqueous precipitation combined with intermolecular polycondensation synthesis of novel HAp porous skeleton material and its Pb²⁺ ions removal performance. *Ceram. Int.* **50**(11), 19757–19768 (2024).
101. Feng, G. et al. Preparation of novel porous hydroxyapatite sheets with high Pb²⁺ adsorption properties by self-assembly nonaqueous precipitation method. *Ceram. Int.* **49**(18), 30603–30612 (2023).
102. Latour, R. A. The Langmuir isotherm: a commonly applied but misleading approach for the analysis of protein adsorption behavior. *J. Biomed. Mater. Res., Part A* **103**(3), 949–958 (2015).
103. Pursell, C. J. et al. Application of the Temkin model to the adsorption of CO on gold. *J. Phys. Chem. C* **115**(48), 23880–23892 (2011).
104. Vigdorowitsch, M. et al. Freundlich isotherm: An adsorption model complete framework. *Appl. Sci.* **11**(17), 8078 (2021).
105. Ezzati, R., *Rethinking the Use of Linear Forms of the Langmuir Isotherm in Adsorption Modeling to Calculate Langmuir Isotherm Parameters* (2023).
106. Li, Z. et al. Empirical likelihood for least absolute relative error regression. *TEST* **23**(1), 86–99 (2014).
107. Narula, S.C. and J.F. Wellington, An overview of the minimum sum of absolute errors regression. *Mathematical programming and game theory for decision making*, pp. 143–167 (2008).
108. Saunders, L. J., Russell, R. A. & Crabb, D. P. The coefficient of determination: What determines a useful R² statistic?. *Invest. Ophthalmol. Vis. Sci.* **53**(11), 6830–6832 (2012).
109. Saha, P. & Chowdhury, S. Insight into adsorption thermodynamics. *Thermodynamics* **16**, 349–364 (2011).
110. Myers, A. L. & Prausnitz, J. M. Thermodynamics of mixed-gas adsorption. *AIChE J.* **11**(1), 121–127 (1965).
111. Alberty, R. A. Calculation of the standard Gibbs free energy, enthalpy, and entropy changes for the hydrolysis of ATP at 0, 25, 37, and 75. In *Horizons of Bioenergetics* 135–147 (Elsevier, 1972).

Acknowledgements

The authors extend their appreciation to the Deanship of Research & Graduate Studies at King Khalid University, KSA, for funding this work through a research group program under grant number RGP. 2 / 574/ 46.

Author contributions

Zahra Sabah Ghnim Writing, Qingling Zhu Laboratory work Ayat Hussein Adhab Khurshed Muzammil Laboratory work Shelesh Krishna Saraswat (Corresponding author) Theory Prakash Kanjariya Supervision Roopashree R Writing Aditya Kashyap Laboratory Work RSK Sharma Laboratory work Piyus Kumar Pathak Theory Morug Salih Mahdi Writing Aseel Salah Mansoor Theory Usama Kadem Radi Figures preparation Nasr Saadoun Abd Laboratory Work Khaled Herati Proofreading submission experimental work.

Declarations

Competing interests

The authors declare no competing interests.

Additional information

Supplementary Information The online version contains supplementary material available at <https://doi.org/10.1038/s41598-025-19112-5>.

Correspondence and requests for materials should be addressed to Q.Z., S.C. or K.H.

Reprints and permissions information is available at www.nature.com/reprints.

Publisher's note Springer Nature remains neutral with regard to jurisdictional claims in published maps and institutional affiliations.

Open Access This article is licensed under a Creative Commons Attribution-NonCommercial-NoDerivatives 4.0 International License, which permits any non-commercial use, sharing, distribution and reproduction in any medium or format, as long as you give appropriate credit to the original author(s) and the source, provide a link to the Creative Commons licence, and indicate if you modified the licensed material. You do not have permission under this licence to share adapted material derived from this article or parts of it. The images or other third party material in this article are included in the article's Creative Commons licence, unless indicated otherwise in a credit line to the material. If material is not included in the article's Creative Commons licence and your intended use is not permitted by statutory regulation or exceeds the permitted use, you will need to obtain permission directly from the copyright holder. To view a copy of this licence, visit <http://creativecommons.org/licenses/by-nc-nd/4.0/>.

© The Author(s) 2025